Comparative Study of Short-term Extreme Responses and Fatigue Damage of Floating Wind Turbines Using Different Blade Models

Xiaoqi Qu[1], Yan Li[1 #], Yougang Tang[1 *], Wei Chai[2,3], Zhen Gao[4]
[1] State Key Laboratory of Hydraulic Engineering Simulation and Safety, School of Civil Engineering, Tianjin University, Tianjin, 300072, China
[2] Key Laboratory of High Performance Ship Technology (Wuhan University of Technology), Ministry of Education
[3] Departments of Naval Architecture, Ocean and Structural Engineering, School of Transportation, Wuhan University of Technology, Wuhan, 430070, China
[4] Department of Marine Technology, Norwegian University of Science and Technology, Trondheim7049, Norway

Abstract: In this work, two different blade structural models are used to estimate the blade deformations and the global structural responses of a 10MW floating offshore wind turbine (FOWT). One model is based on the Euler-Bernoulli beam theory and it is solved by the linear normal mode superposition method. The other model is based on the geometry exact beam theory (GEBT) which can consider the full geometric nonlinearity and large deformation. The control equations of GEBT are discretized by Legendre spectral finite elements. The aero-hydro-servo-elastic fully coupled numerical simulations are conducted in the open-source analysis tool OpenFAST to explore the feasibility of the two different structural models for modeling large scale wind turbine blades. Both the steady-state and dynamic results show that power generation and thrust on rotor are similar for the different blade models. There is a small difference in the results of the blade pitch angle and flapwise and edgewise blade root bending moment at high wind speeds due to the lack of torsion degree of freedom in the mode-based method. The difference between the two models is mainly reflected in the prediction of blade tip deformations. The one-hour short-term extreme blade root bending moments and the damage equivalent fatigue loads at blade root are both compared based on the two models. For edgewise bending moment, the extreme value of GEBT model is found at cut-out wind speed, whereas the linear beam model predicts the extreme value around rated wind speed. For the flapwise bending moment, the extreme value is captured around the rated wind speed for both of the two models, but GEBT model presents a larger value. As for fatigue loads, the short-term 1Hz damage equivalent loads calculated based on the linear

* Corresponding author. Email: tangyougang_td@163.com
# Co-corresponding author. Email: liyan_0323@tju.edu.cn

beam model are smaller than GEBT model at almost all load cases for both edgewise and flapwise root bending moment, which implies that the linear beam model may underestimate the life time fatigue damage at blade root.

Keywords: wind turbine blade; 10MW FOWT; structural model; short-term extreme load response; damage equivalent fatigue loads.

1. Introduction

The global cumulative installed wind capacity is growing rapidly in recent years. Global wind report forecasts over 300GW capacity to be added in the next 5 years [1]. The growth mainly comes from emerging markets and offshore wind. Nowadays, the capacity of a single offshore wind turbine (OWT) is tending to be increased to reduce the wind energy costs. Modern large wind turbine blades can be regarded as long slender structures suffering from gravity, centrifugal force, and aerodynamic force [2]. These forces lead to complex and large elastic structural deformation of the long flexible blades. Meanwhile, composite materials of high stiffness-to-weight ratio are used in production to decrease the weight of blades. Thus the dynamic responses of large rotating blades can be characterized both geometric nonlinearities and material nonlinearities [3]. As one of the most significant parts for wind turbine system, it is crucial to precisely simulate and analyze the blade dynamic responses under varied environmental conditions, especially for extreme structural load responses and fatigue damage.

Blades on modern large wind turbines are generally made of thin-walled beams with composite materials. Due to the intrinsic nature of composite materials and the complexity of blade structural topologies [4], it is quite challenging to choose an accurate and efficient numerical model to capture the elastic coupling effects of blades. Comparing with the 3D structural analysis based on shell or solid model [5], beam models are sufficiently accurate and computationally efficient for wind turbine blade structural analysis. In some studies [6, 7] as well as widely used numerical software, such as Bladed [8] and the ElastoDyn module in FAST [9], the blade is modeled as a simple Bernoulli-Euler beam. And the blade dynamic responses are calculated based on an assumed mode method without consideration of torsion deformation and bend-twist coupling effect.

However, former research works show that torsion deformation has a significant effect on blades dynamic responses, especially the flutter instability [10, 11]. Although some of the aforementioned researches considered geometric nonlinearities in blade dynamic analysis, the mode superposition method used to linearize the control equations of blade motion is limited to moderate deflections which may be not feasible to large scale blades. Recently GEBT is diffusely employed to model the highly flexible wind turbine blades [11-13]. Based on this model, geometric nonlinearity and large deflection can be fully considered.

Among the studies on bend-twist coupling effect of blades, almost all of them focused on the 5MW wind turbine, while few works have been performed on 10MW or even larger scale ones. The aero-elastic code HAWC2 is frequently used to model 10MW wind turbine [14], but it is based on a combined multi-body method where geometric constraint equations need to be solved separately. In contrast, the GEBT model in FAST can enable full geometric nonlinearity with a single finite element [12]. Considering the development and application of large-capacity FOWTs, it is necessary to explore the differences between the various methods implemented in structural analysis for large highly flexible blades.

In addition to structural modeling, ultimate limit state (ULS) analysis is an important consideration for the safety of FOWT blades. Estimating extreme loads for wind turbine blades is made effectually difficult by the nonlinear nature of the wind turbine physics combined with the stochastic nature of the wind and wave input [15]. Because extreme loads are compactly related to the requirements of blade materials and further the wind turbine costs, it is vital to obtain the extreme loads of FOWT blades accurately. However, direct calculation of extreme loads usually needs an unimaginable large number of simulations which quantity is hardly applicable.

According to the IEC standard 61400-3[16], the ultimate loads acting on the offshore wind turbine is required to be calculated through statistical extrapolation of the load response results of multiple simulations. However, the extrapolation procedure is not precisely provided in the standard. Many statistical extrapolation approaches are hereby proposed and compared in recent studies. Barone et al. [17] performed simulations of a 5MW wind turbine ninety-six years operation to obtain a large database of wind turbine loads, including extreme loads and fatigue cycles. The tail of the distribution was well behaved providing confidences in extrapolation method with limited simulation data. Xia and Wang [18] compared different extreme load extraction methods used for extreme load prediction. They also fitted the Gumbel distribution as recommended in the IEC standard 61400-1 [19] to evaluate the extreme load of blade root out-of-plane bending moment for fixed and floating offshore wind turbine. The results showed that the block maximum and the peak-over-threshold (POT) method are better than the global maximum method. Similar conclusions were also found in Lott and Cheng's study [20]. Apart from that, they also compared the statistical distribution functions as well as the fitting methods in order to estimate the extreme loads based on measurements from an offshore wind turbine. As for the tower base fore-aft bending moment, the POT method, the 3-parameter Weibull distribution and the maximum likelihood method were recommended for the best approximation to the measurement data. The extrapolation techniques were widely used in estimating the extreme loads of wind turbine system and similar works can also be found in [21-24].

Although many efforts have been devoted to study the extreme structural responses for wind turbines, most of these works focused on onshore or medium scale offshore wind turbine. There are few published works regarding extreme load responses analysis for large scale FOWTs. The longer and more flexible wind turbine blades can generate larger and more complex deformation which may result in severer extreme structural load responses. Thus in present study, the extreme blade structural responses induced by stochastic wave and wind were investigated for DTU 10MW reference wind turbine (RWT) mounted on a floating platform. The simulations used to extrapolate for the extreme load responses were performed by the aero-hydro-servo-elastic fully coupled analysis tool OpenFAST developed by the National Renewable Energy Laboratory (NREL). Two different methods were used to model the wind turbine blade and the dynamic responses were compared. The source code related to the control module was recompiled for a 64-bit application. The extreme structural load responses were obtained by Naess-Gaidai method or up-crossing rate method which is proved better than Gumbel method[25]. Furthermore, the short-term damage equivalent fatigue loads for blade root bending moments were also evaluated based on the time series calculated by the two structural models to perform a more comprehensive comparison.

This paper is structured as follows. In Section 2, the key parameters of the DTU 10MW FOWT system are introduced. This is followed by the methodology described in Section 3, including the methods used for different blade structural models, fully coupled dynamic analysis, extreme value estimation, short-term damage equivalent loads calculation and the validation of established FOWT model. In Section 4, the steady-state results from a wind ramp simulation are compared and analyzed. After the environmental conditions and load cases are defined in Section 5, the comparative studies for different blade models and short-term extreme structural responses under stochastic wind and wave, as well as the short-term damage equivalent fatigue loads for blade root bending moments are provided in Section 6.

2. DTU 10MW FOWT

In this study, the DTU 10MW RWT mounted on a newly designed semi-submersible floater is employed for numerical simulation (see Figure1). The original DTU 10MW RWT is designed for operating under IEC class 1A wind climate, but in this work, the climate is changed to IEC Class 1C according to reference [26]. The key parameters of the wind turbine are listed in Table 1, and more details can be found in [27]. Specifically, the rotor diameter of the RWT is 178.3m and the length of a single blade is up to 86.466m, which is about 20 meters longer than the NREL 5MW wind turbine blade. It is worth noting that the tower has been modified for adapting the wind floater.

The numerical model of OO-Star Wind Floater employed in the LIFES 50+ Project [28] for supporting the 10MW RWT is established in this study by DNV software SESAM (see Figure2). The semi-submersible floater is composed of a central column and three outer columns with a cylindrical upper part and a tapered lower part. All these columns are mounted on a three-legged, star-shaped pontoon with a bottom slab. The floater is moored by three catenary mooring lines as shown in Figure 3. A clump mass is attached to each line, separating the line in two segments. The upper segment, which is connected to the fairlead, is 160 m long. The lower segment is 543 m long. The main properties of the mooring system are listed in Table 3, and more details about this floating system are extensively introduced in references [28] and [29].

Figure 1 The OO-Star Wind Floater Semi 10MW concept [29]

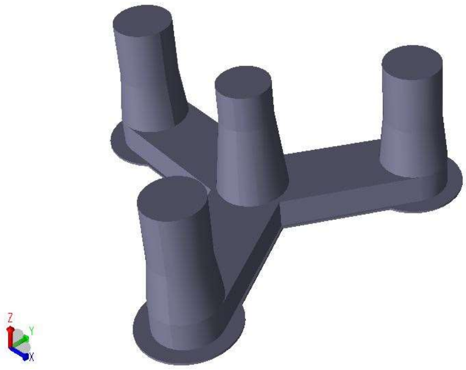

Figure 2 LIFES50+ OO-Star Wind Floater structure

Table1 Key parameters of the DTU 10 MW Reference Wind Turbine [27]

Parameters	Value
Rated power	10MW
Rotor orientation, Configuration	Upwind, 3 blades
Rotor Diameter	178.3m
Cut in, rated and cut out wind speed	4m/s, 11.4m/s, 25m/s
Hub Diameter and Hub Height	5.6m, 119.0m
Minimum and Maximum Rotor Speed	6.0rpm, 9.6rpm
Rotor Mass	227,962 kg
Nacelle Mass	446,036 kg
Tower Mass [28]	1,257,000kg

Table2 LIFES50+ OO-Star Wind Floater Semi 10MW platform parameters [28]

Property	Value
Overall substructure mass (excl. tower, mooring)	2.1709E+07 kg
Centre of Mass (CM) below MSL	15.225 m
Substructure roll inertia about CM	9.43E+09 kg·m^2
Substructure pitch inertia about CM	9.43E+09 kg·m^2
Substructure yaw inertia about CM	1.63E+10 kg·m^2
Tower base interface above MSL	11.0 m
Draft at equilibrium position with moorings	22.0 m
Displaced water volume(including ballast)	2.3509E+04 m^3
Centre of buoyancy below MSL	14.236 m

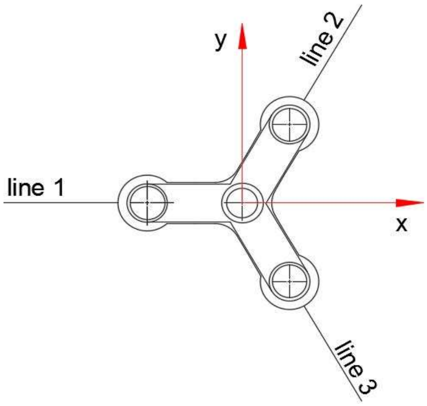

Figure3 Arrangement of mooring line

Table3 mooring system properties[28]

Property	Value
Number of lines	3
Angle between adjacent lines	120 deg
Vertical position of fairleads above MSL	9.5 m
Radius to fairleads from platform centerline	44 m
Vertical position of anchors below MSL	130.0 m
Radius to anchors from platform centerline	691 m
Equivalent mass per length in air	375.38 kg/m
Extensional stiffness EA	1.506E+09 N
Effective hydraulic diameter of the chain	0.246 m

3. Methodology

3.1 Fully coupled numerical model

The open-source computer-aided engineering tool OpenFAST is implemented in this study. This code is developed by researchers at the NREL. The comprehensive aero-hydro-servo-elastic analysis tool is capable for simulating the coupled dynamic responses of both onshore and offshore wind turbines under varied environmental conditions. The numerical model of state-of-the-art 10MW FOWT was originally established by FAST v8.16.00a-bjj in the LIFE50+ Project [26]. The blade and tower are modeled as a cantilever beam, and the deflection of the structures is solved based on the assumed-mode method. The definition of the coordinate systems are illustrated in Figure4. $OXYZ$ represents the global inertial coordinate system. And $o_{b,j}x_{b,j}y_{b,j}z_{b,j}$ is the local coordinate system for blade j, which is defined according to the IEC standard[19]. $z_{b,j}$ axis points along the pitch axis towards the tip of blade j. $y_{b,j}$ axis points towards the trailing edge of blade j and parallel with the chord line at the zero-twist blade station[9]. $x_{b,j}$ axis is orthogonal with $y_{b,j}$ and $z_{b,j}$ axis. The aerodynamic loads are calculated based on blade element momentum theory, while the hydrodynamic loads are obtained by potential flow theory. The dynamic effects and hydrodynamic loads of the multi-segment mooring lines are estimated by lumped-mass approach.

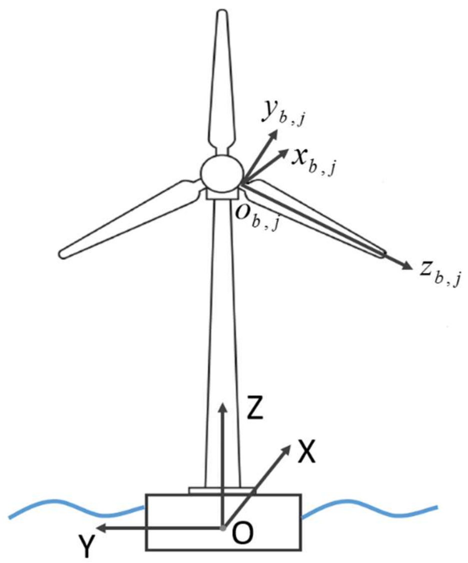

Figure 4 Global and blade local coordinate systems

Although a lot of simulations and analysis were carried out to prove the applicability of the proposed 10MW FOWT model in the LIFES 50+ Project, few of them focus on the accuracy of the blade structural model, which ignored the torsion deformation for simulating large-scale wind turbine blades dynamic responses. Besides, the torsion deformation and bend-twist coupling effect which have an appreciable influence on aero-elastic responses and stability of wind turbine blades [30] are not included in the above studies. Thus, it is necessary to investigate the variance of different blade structure models and their effect on the dynamic responses of the whole system.

3.2 Blade models

In the current version of OpenFAST code, there are two modules to calculate the deformation and dynamic responses of the blades, which are ElastoDyn and BeamDyn, respectively. The methodologies of both modules are described in the following sections.

3.2.1 ElastoDyn blade structural model

In the ElastoDyn FAST module, the blade is modeled as a flexible cantilevered beam with continuously distributed mass and stiffness. The beam is straight and isotropic without cross-sectional couplings and torsion and shear effects. The normal mode superposition method is used to reduce the number of degree of freedoms (DOFs) from infinity to *n*, the number of normal modes considered to be dominant [31]. Then the deflection of any point on the beam can be expressed as a linear sum of the normal mode shapes:

$$u(z,t)=\sum_{a=1}^{n}\phi_a(z)q_a(t) \tag{1}$$

where $u(z,t)$ is the lateral deformation at time t and location z. $\phi_a(z)$ and $q_a(t)$ are the normal mode shape and generalized coordinate for normal mode a, respectively.

Alternatively, the lateral deflection of the flexible beam could also be expressed using n other functions, $\phi_b(z)$, not unique to each normal mode[31]:

$$u(z,t)=\sum_{b=p}^{n+p-1}\varphi_b(z)c_b(t) \tag{2}$$

where $c_b(t)$ is the generalized coordinate associated with the shape function φ_b. p is a parameter chosen for convenience.

According to the Rayleigh-Ritz method, each normal mode of the beam can be obtained by the combination of the n shape functions with the constant proportionality coefficient $C_{a,b}$:

$$\phi_a(z)=\sum_{b=p}^{n+p-1}C_{a,b}\varphi_b(z) \tag{3}$$

In the ElastoDyn module, the polynomial is selected as the shape function. Thus the b^{th} shape function is defined as:

$$\varphi_b(z)=\left(\frac{z}{Z}\right)^b, \tag{4}$$

The coefficients $C_{a,b}$ can be solved by the following equation:

$$(-\omega_a{}^2\mathbf{M}_{n\times n}+\mathbf{K}_{n\times n})\mathbf{C}_{\mathbf{a}\,n\times 1}=\mathbf{0}_{n\times 1} \tag{5}$$

where $\mathbf{M}_{n\times n}$ and $\mathbf{K}_{n\times n}$ are the generalized mass matrix and stiffness matrix. The n roots $\omega_a{}^2$ are the square of the natural frequency associated with normal mode a [31]. In the numerical simulations, p is set to 2 and n is set to 5. Meanwhile, the first and second flapwise modes as well as the first edgewise mode is considered. The torsion deformation is not included in the ElastoDyn module.

3.2.2 BeamDyn blade model

As ElastoDyn module is not capable to capture the full geometric nonlinearity of highly flexible, composite wind turbine blades [12]. Recently, a new time-domain structural-dynamics module, BeamDyn, is developed for slender structures. Based on geometrically exact beam theory (GEBT), this new module provides capabilities for modeling initially curved and twisted composite wind turbine blades undergoing large deformation, including bending, torsion, shear, and extensional DOFs [32]. Legendre spectral finite elements (LSFEs) are used to discretize the GEBT beam equation in space domain. In this study, a single 5th order LSFE with 51 cross-section stations is employed to calculate the dynamic responses of wind turbine blades. The governing equations of motion for GEBT can be written as [3]

$$\dot{\underline{h}} - \underline{F}' = \underline{f}, \tag{6}$$

$$\dot{\underline{g}} + \tilde{\dot{u}}\,\underline{h} - \underline{M}' + (\tilde{x}'_0 + \tilde{u}')^T \underline{F} = \underline{m}, \tag{7}$$

where $\underline{h}$ and $\underline{g}$ are the linear and angular momenta resolved in the inertial coordinate system, respectively; $\underline{F}$ and $\underline{M}$ are the beam's sectional force and moment resultants, respectively; $\underline{u}$ is the one-dimensional (1D) displacement of a point on the reference line; x_0 is the position vector of a point along the beam's reference line; and $\underline{f}$ and $\underline{m}$ are the distributed force and moment applied to the beam structure.

After linearization and finite element implementation the governing equations can be expressed by [3]:

$$\underline{\underline{\hat{M}}}\Delta\underline{\hat{a}} + \underline{\underline{\hat{G}}}\Delta\underline{\hat{v}} + \underline{\underline{\hat{K}}}\Delta\underline{\hat{q}} = \hat{F}^{ext} - \hat{F} \tag{8}$$

where $\underline{\underline{\hat{M}}}$, $\underline{\underline{\hat{G}}}$ and $\underline{\underline{\hat{K}}}$ are the elemental mass, gyroscopic and stiffness matrices, respectively, and $\underline{\underline{\hat{F}}}$ and $\underline{\underline{\hat{F}}}^{ext}$ are the elemental forces and externally applied loads, respectively. $\Delta\underline{\hat{q}}$, $\Delta\underline{\hat{v}}$, and $\Delta\underline{\hat{a}}$ are the increment of nodal values for the displacement, velocities, and accelerations, respectively. These matrixes can be obtained by integrating the sectional parameters multiplied by shape functions in an elemental. For example:

$$\underline{\underline{\hat{M}}} = \int_0^l \underline{\underline{N}}^T \underline{\underline{M}}^I \underline{\underline{N}} dx_1 \tag{9}$$

where $\underline{\underline{N}}$ is a matrix storing the spectral basis functions obtained by p^{th}-order Lagrangian interpolation and $\underline{\underline{M}}^{I}$ is the sectional mass matrix resolved in inertial system.

The BeamDyn module can model initially curved and twisted composite wind turbine blades, while the ElastoDyn module can only be applied to straight isotropic blades. The BeamDyn module has the ability to consider full geometric nonlinearity and large deflection with bending, torsion, shear and extensional DOFs. However only flapwise and edgewise bending deformation are calculated in the ElastoDyn module. Figure 5 shows the blade deformation modeled by the two different structural models. The frames $x_1y_1z_1$ and $x_2y_2z_2$ in the figure represent the local coordinate system of blade cross-section in ElastoDyn and BeamDyn module respectively. Previous work has proven that the results given by BeamDyn model agree better with the field measurements for the aeroelastically tailored curved blades of a 2.3MW onshore wind turbine [33].

Although the high-fidelity BeamDyn module can capture the complicated and large deformation of long flexible composite blades, it always needs a relatively small time step to converge the solution. For example, in this study, the time step adopted in BeamDyn module is 0.001s, while that of ElastoDyn module is 0.025s. Therefore, for the simulations under the same environmental scenario, the realistic computing time of BeamDyn module is about 20 times as that of ElastoDyn module. Hereby, it is significant to balance the accuracy of blade response prediction and computing efficiency. The conclusion of this study can provide guidance for future work. For example, the linear mode superposition method can be used to study the responses, which are not sensitive to the blade torsion deformation, to improve computing efficiency. However, as for the responses, which are closely related to bend-twist coupling effect, should employ higher order structural model.

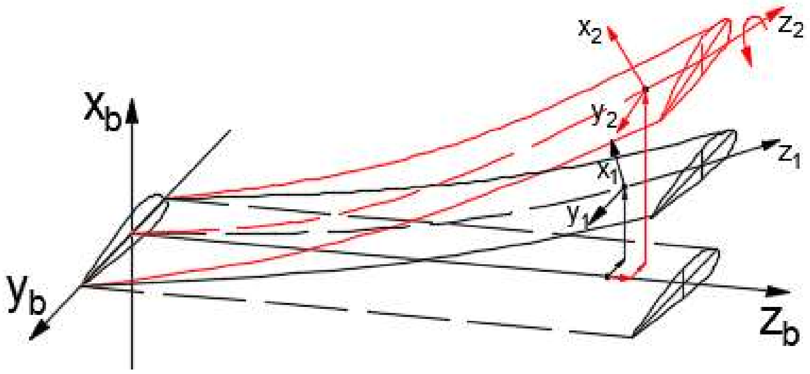

Figure 5 Schematic of the beam deformation based on different structural models (Black blade for ElastoDyn model, red blade for BeamDyn model)

3.3 Extreme value estimation of blade root bending moment

In this study, the one-hour short-term extreme blade root bending moment is estimated based on the aforementioned two different structural models. As one of the key parameters for estimation of the large and extreme response statistics, the mean up-crossing rate is widely used for evaluation of the associated reliability of marine structures [25]. In this work, the mean up-crossing rate method is implemented to estimate the extreme structural responses.

The sample mean up-crossing rate $\hat{v}^{+}(\zeta)$ can be obtained from the simulated time series by the following expression [34]:

$$\hat{v}^{+}(\zeta) = \frac{1}{kT}\sum_{i=1}^{k} n_i^{+}(\zeta, T), \tag{10}$$

where $n_i^{+}(\zeta, T)$ denotes the counted number of up-crossing of the level ζ within a time duration of length T for simulated i-th time history. k is the total number of simulations. An appropriate approximation of the 95% confidence interval ($\mathrm{CI}_{0.95}$) for the mean up-crossing rate can be calculated according to the following equation:

$$CI_{0.95}(\zeta) = \left(\hat{v}^{+}(\zeta) - 1.96\frac{\hat{s}(\zeta)}{\sqrt{k}}, \hat{v}^{+}(\zeta) + 1.96\frac{\hat{s}(\zeta)}{\sqrt{k}}\right), \tag{11}$$

where the empirical standard deviation $\hat{s}(\zeta)$ can be expressed by

$$\hat{s}(\zeta)^2 = \frac{1}{k-1}\sum_{i=1}^{k}\left(\frac{n_i^{+}(\zeta;T)}{T} - \hat{v}^{+}(\zeta)\right)^2 \tag{12}$$

If the assumption of statistically independent up-crossing is valid at high response levels, it is reasonable to assume that the random number of up-crossing in an arbitrary time interval of length T is approximately Poisson distributed. Therefore, the extreme value of blade structural responses can be written as $M(T)=\max\left\{Y(t):0\le t\le T\right\}$, where $Y(t)$ is the blade structural responses over the time interval of length *T*. Then the cumulative distribution function (CDF) of $M(T)$ is given as [25]

$$\mathrm{P}(M(T)\le\zeta)=\exp(-v^{+}(\zeta)T), \tag{13}$$

and the exceedance probability of a defined level ζ is given as follows:

$$\mathrm{P}(M(T)>\zeta)=1-\exp(-v^{+}(\zeta)T), \tag{14}$$

For the far tail region, as the conventional Monte-Carlo Simulation method is inefficient for calculating the mean up-crossing rate, the extrapolation technique is usually used to predict the extreme response. For the dynamic responses of offshore structures, including FOWTs, the mean up-crossing rate $\hat{v}^{+}(\zeta)$ is in general highly regular in a specific way in the tail region. In fact, according to a large class of stochastic process, the mean up-crossing rate tail (e.g. $\zeta\ge\zeta_0$) behaves similarly to $\exp\left\{-a(\zeta-b)^{c}\right\}$, where $a>0$, $b\le\zeta_0$, and $c>0$ are suitable constants. Therefore, as discussed in detail in Naess and Gaidai [35], the mean up-crossing rate in the tail region is approximated as

$$v^{+}(\zeta)\approx q(\zeta)\exp\left\{-a(\zeta-b)^{c}\right\},\ \ \zeta\ge\zeta_0 \tag{15}$$

where the function $q(\zeta)$ is slowly varying, compared with the exponential function $\exp\left\{-a(\zeta-b)^{c}\right\}$ in the tail region. And for large values of ζ, the function $q(\zeta)$ can be replaced by a constant *q*. The optimal values of parameters *a*, *b*, *c* and *q* can be determined by minimizing the logarithmic level mean square error function,

$$F(q,a,b,c)=\sum_{j=1}^{N}\rho_j\left|\ln\hat{v}^{+}(\zeta_j)-\ln q+a(\zeta_j-b)^{c}\right|^{2}, \tag{16}$$

where $\hat{v}^{+}(\zeta_j), j=1,\ldots N$ is a set of empirical mean up-crossing rates at different levels. ρ_j is the corresponding weight factor and we use $\rho_j=(\ln CI^{+}_{0.95}(\zeta_j)-\ln CI^{-}_{0.95}(\zeta_j))^{-2}$ in this work . The Levenberg-Marquardt least squares optimization method is employed to solve the optimal values for a, b, c and q. More details of this method can be found in references [34] and [35].

Due to the regularity of the mean up-crossing rate in the tail region, extreme value statistics can be calculated with the assistance of the abovementioned extrapolation technique. The empirical estimation of the up-crossing rate with respect to the far tail region can be achieved satisfactorily with much less computational efforts than the traditional Monte Carlo Simulation method.

3.4 Short-term fatigue damage evaluation of blade

The wind turbine system suffers from the stochastic wind and wave loads which can lead oscillations of blade structural responses. To conduct a more thoroughly comparison, the short-term fatigue damage of the blade root was evaluated based on the NREL code MLife [36]. The short-term damage equivalent loads (DELs) for blade root bending moment were calculated according to the time series obtained by the aforementioned blade structural models. A DEL is a constant-amplitude fatigue-load that occurs at a fixed load-mean and frequency and produces the equivalent damage as the variable spectrum loads[36]. MLife can compute a short-term, time-series-based DEL by

$$DEL_j^{ST} = \left(\frac{\sum_i (n_{ji} (L_{ji}^R)^m)}{n_j^{STeq}} \right)^{\frac{1}{m}} \tag{17}$$

$$n_j^{STeq} = f^{eq} T_j \tag{18}$$

where DEL_j^{ST} and L_{ji}^R are the DEL and cycle' load range for time-series j about a fixed mean, respectively. n_{ji} is the cycle count. Here the rain-flow counting algorithm is employed to calculate for the n_{ji}. m is the Whöler exponent which is determined by the S-N curve of the material under consideration. According to the DTU report[27], m is set to 10 for blade root. f^{eq} is the DEL frequency, which is set to 1Hz in this study. T_j and n_j^{STeq} are the elapsed time and total equivalent fatigue counts for time-series j, respectively.

3.5 Validation of free decay test for blade and tower

The numerical model of the DTU 10MW FOWT was established in OpenFAST. And the free decay simulations were performed to predict the natural frequencies of the blades and tower. By comparing the results among different models and codes, the accuracy and robustness of present model is firstly verified. It should be mentioned that the floater motion and mooring system are not included in the free decay model for simplification, since the major focus is on the accuracy of the blade structural models in BeamDyn and

ElastoDyn. The initial displacements of free decay simulations were chosen based on the descriptions in the DTU report [37]. To be specific, a five-meter displacement in the fore-aft direction was applied on the tower top. The total simulation duration is 300s. According to the Fast Fourier Transformation, the natural frequencies are calculated and listed in Table 4. During the simulation, the rotor is parked. Therefore, aerodynamic loads are not applied to the blades. The spectral responses of blade tip displacement and tower top displacement are presented in Figure 6. The results are also compared with HAWC2 predictions presented in [37].

The agreement in natural frequencies between BeamDyn, ElastoDyn, and HAWC2 is close enough to ensure the accuracy of the 10MW wind turbine models in OpenFAST. Some dominant frequencies, which are listed and compared in Table 4, can also be identified in the figure. Furthermore, it can be found that BeamDyn can accurately capture some high-frequency components, which do not occur in ElastoDyn. The similar conclusion is also obtained in reference [33, 38].

Table 4 Natural frequencies for the isolated blade

Mode description	FAST(ElastoDyn)	FAST(BeamDyn)	Difference(%)	HAWC2
1st tower fore-aft and side-side mode	0.248 Hz	0.247 Hz	0.40	0.251 Hz
1st collective blade flap mode	0.637 Hz	0.630 Hz	1.10	0.630 Hz
1st asymmetric blade edge mode	0.987 Hz	0.923 Hz	6.48	0.935 Hz

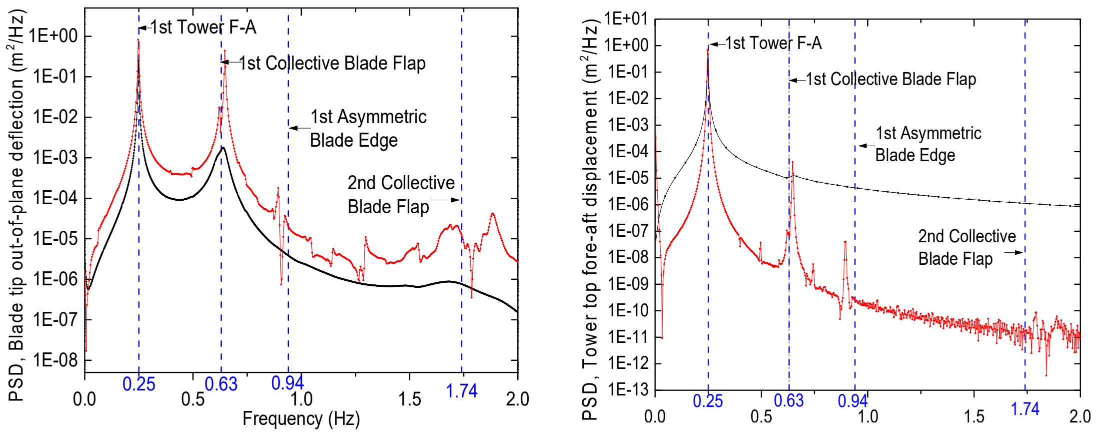

(a)PSD of blade tip out-of-plane deflection (b)PSD of tower top fore-aft displacement

Figure 6 Results for tower top free decay simulation (black line: FAST(ElastoDyn), red line: FAST(BeamDyn), blue dash line: HAWC2)

4. Results for constant and uniform wind field with no waves

In this part, the whole FOWT model, including the floating platform and mooring system, is implemented to evaluate the global steady-state performance. Without waves, the uniform, steady wind speed changing in intervals of 1 m/s was applied every 10 min from cut-in wind speed 4 m/s to cut-out wind speed 25 m/s, see Figure 7a. The original DTU controller was modified and recompiled for application in 64-bit OpenFAST. From Figure 7b to 7d, it is seen that the new controller performs well in the aspect for regulating rotor speed and blade pitch as wind speed changing. On one hand, the rotor speed is regulated to obtain the optimized electrical generator power when wind speed is lower than the rated. On the other hand, once the 10MW rated power is reached, the blade pitch angle is adjusted to remain the rated power output under high wind speed cases, and this will also lead to decrease of the aerodynamic load on the rotor, see Figure 7g.and 7h.

For the two different blade structural models, the rotor performs similarly, including rotor speed in Figure 7b and blade pitch angle in Figure 7c. To be specific, in the range of low wind speeds, the rotor speed keeps as a constant of 6 rpm. Then it begins to increase at the wind speed of 8 m/s until reach the rated value of 9 rpm and remains unchanged. Furthermore, as shown in Figure 7c the blade pitch angle shows a small difference for the two structural models at high wind speeds. ElastoDyn module requires a relatively larger pitch angle compared to BeamDyn module. The difference is mainly due to the lack of blade torsional deformations in ElastoDyn.

As wind speed increases, the torsional effect becomes more important. In Figure 7e-7h, apparent differences between the results calculated by the two models can be observed at above-rated wind speeds. It is noteworthy that when the control system begin to pitch the blade, the edgewise blade tip deformation and root bending moment both show a great changes of the response value. In other words, the torsional deformation and blade pitch motion have a significant effect on blade edgewise responses. Previous work has shown that the bend-twist coupling effect closely related with the blade stability[30]. While these coupling effects can be well studied by BeamDyn module instead of ElastoDyn.

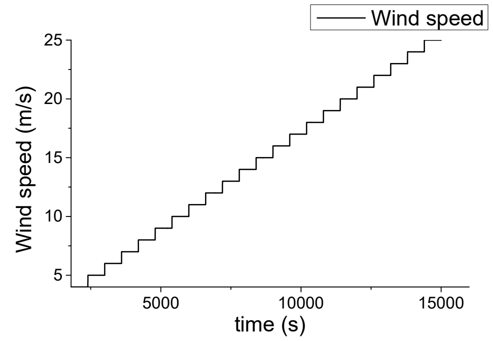

(a) step wind speed

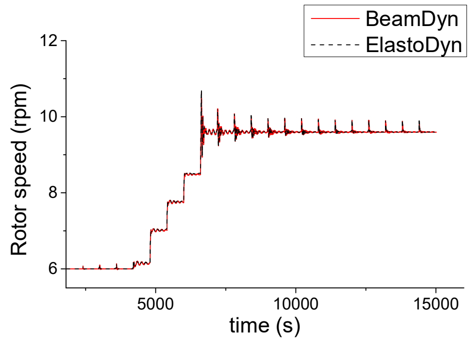

(b) rotor speed

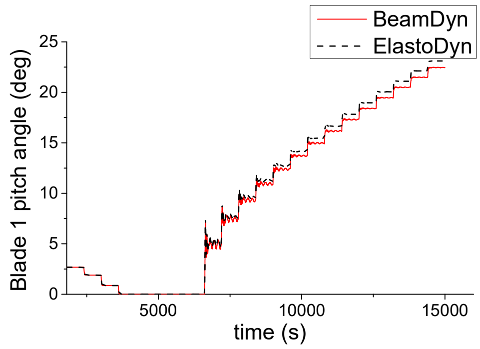

(c) Blade 1 pitch angle

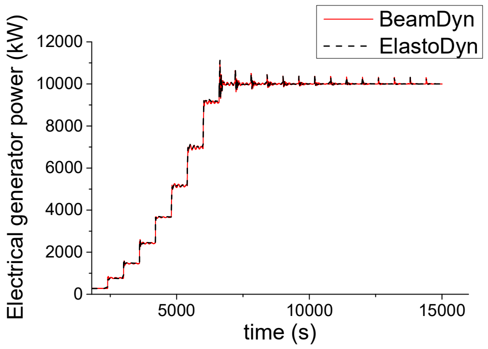

(d) Electrical generator power

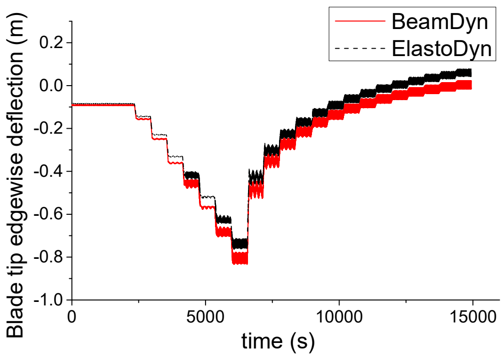

(e) blade tip edgewise deflection

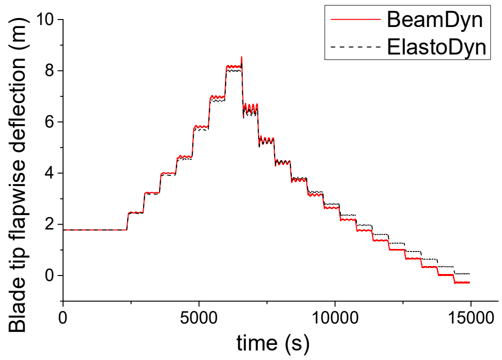

(f) blade tip flapwise deflection

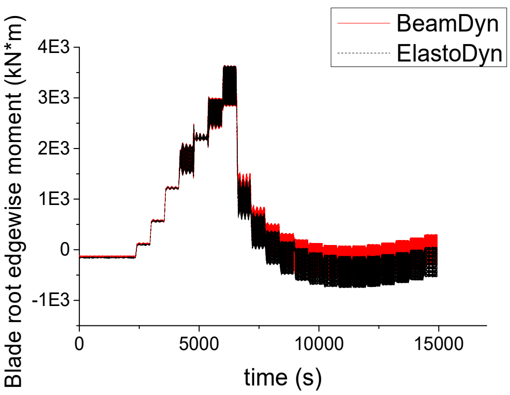

(g)blade root edgewise bending moment

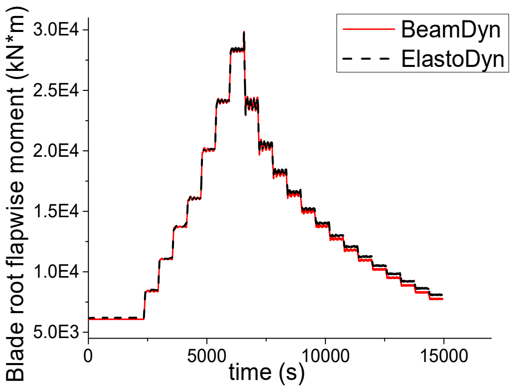

(h)blade root flapwise bending moment

Figure 7 Responses to step uniform wind

5. Description of environmental conditions and load cases

A series of representative load cases (LCs) are defined in Table 5 for the time domain simulations of FOWT system. The target sea site is selected at the Gulf of Maine with a water depth of 130 m and associated environmental parameters are specified in [39].

The power law profile was used accordingly to the recommendations stated in DNV-OS-J101[40] to calculate the 10 minutes mean wind speed at a reference height as below

$$u_{10}(z_{ref}) = u_{10}(z_0)(\frac{z_{ref}}{z_0})^{0.14} \tag{19}$$

The reference height z_{ref} is set as 119m, the height of the hub above mean sea level (MSL). $u_{10}(z_0)$ is the measured mean wind speed at z_0 height above MSL. TurbSim is used to generate three-dimensional turbulent wind fields. The normal Kaimal spectrum and exponential coherence model for IEC Class C is set as turbulence model and the scaling from the IEC 61400-3 [16] is used. The stochastic wave is modeled by the Pierson-Moskowitz spectrum. The corresponding parameters, including the significant wave height, Hs and the peak period, Tp are selected based on the joint probability distribution of occurrence sea state in the selected Gulf of Maine site. Besides, the directions of wind are wave aligned. Each simulation is run for 5400s, and the first 1800s result is removed to eliminate transient effect given by the long surge natural period of floating platform [29]. To provide reasonable simulation results, five seeds of turbulent wind and irregular wave samples were taken for each LC.

Table 5 Environmental condition [26]

	V_{wind}	H_s	T_p	Duration
Load case 1	5.0 m/s	1.38 m	7.0 s	5400 s
Load case 2	7.1 m/s	1.67 m	8.0 s	5400 s
Load case 3	10.3 m/s	2.20 m	8.0 s	5400 s
Load case 4	13.9 m/s	3.04 m	9.5 s	5400 s
Load case 5	17.9 m/s	4.29 m	10.0 s	5400 s
Load case 6	22.1 m/s	6.20 m	12.5 s	5400 s

Load case 7	25.0 m/s	8.31 m	12.0 s	5400 s

6. Results and discussion

The responses of FOWT predicted by two different blade structural models under stochastic wind and wave are compared. The statistical data are presented including the mean value, standard deviation, maximum and minimum values of FOWT system responses in each LC, and these values are calculated based on the average value of the five identical and independent simulations. The standard deviation of the time series is plotted as the error bar. The value of error bar is obtained through mean value adding and subtracting one standard deviation.

Firstly, the power output and the thrust force of the wind turbine are compared. Because the only difference between the two numerical models is the method employed to model the blade structure, there are very little changes in the global responses such as floater motions, mooring lines tension and tower base bending moments. Thus, the comparison is focused on the blade structural dynamic responses such as blade root bending moment and tip deflection in the time and frequency domains. Through these comparisons, the effect of blade torsion deformation and bend-twist coupling on different dynamic responses can be investigated. Furthermore, the one-hour short-term extreme structural responses and the 1Hz short-term DELs for blade root bending moment are also calculated based on the method proposed in Section 3.3 and 3.4.

6.1 Comparison of FOWT system global responses

In this part, the power production performance of the two different models is studied. Figure 8 shows the statistical data of electrical generator power for the two models. The mean value of the electrical generator power shows the same trend as that in Figure 7d, which proves the effectiveness of the controller in both steady and stochastic states. The error bar in the figure represents the standard deviation of the time series of power generation in each load case. The maximum and minimum instant value during the simulations are also plotted. Overall, the results of power generation are almost same for these two models. To be specific, the difference of the mean value between the two models is below 1%. Therefore, with the advantage of higher calculation efficiency, the ElastoDyn module is more recommended to evaluate the power production performance of FOWT. In addition, it is worthy to mention that the standard deviation of LC3 is significantly greater than other cases. This phenomenon is caused by the transition from partial to full load operation, where the rotor speed is specifically sensitive to the wind speed and further affect the power generation.

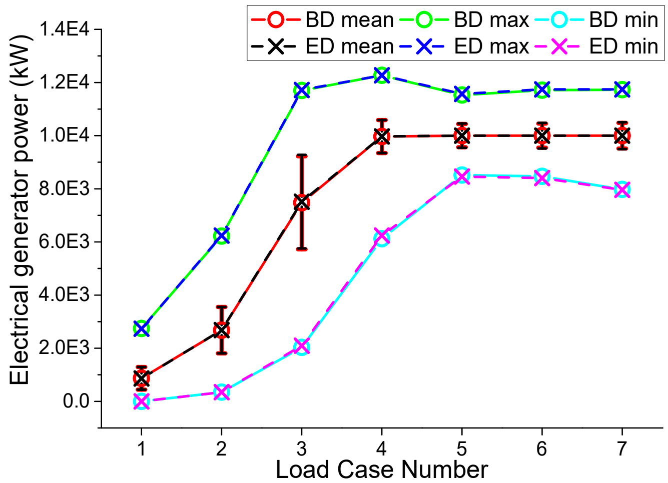

Figure 8 Statistical data of electrical generator power dynamic results

In Figure 9, the comparative study on rotor thrust between the two models is conducted. One can observe that both mean values and standard deviations of these two models have almost no difference with each other in most of the cases. Although the BeamDyn results are a little larger at high wind speeds, the minor differences can be neglected. Thus for the study of rotor thrust, between the cut-in and cut-out wind speeds, the ElastoDyn OpenFAST module should be adopted to model the blade structure for higher computational efficiency.

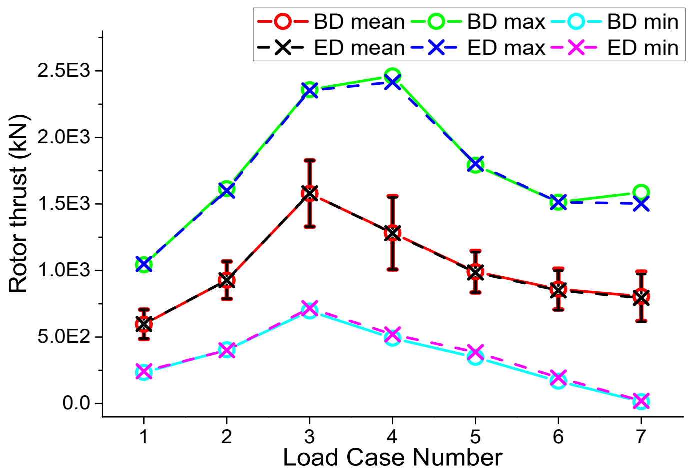

Figure 9 Statistical data of rotor thrust dynamic results

The comparison of blade 1 pitch angle obtained by the two different structure models is presented in Figure 10. It is obvious that the ElastoDyn module shows a higher blade pitch angle than BeamDyn at all LCs. It is due to the lack of blade torsional deformation in ElastoDyn module. At high wind speeds, the difference is more evident. Thus for the study of FOWT control system, it is better to employ the BeamDyn module which can consider the torsional deformation of the blade and predict a more precise blade pitch angle.

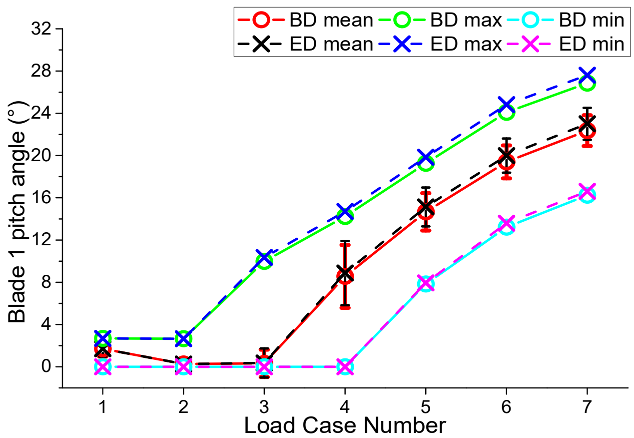

Figure 10 Statistical data of blade 1 pitch angle results

6.2 Comparison of blade tip deflections

6.2.1 Statistical results

Blade is one of the key components in wind turbine system for capturing wind energy. Generally, a wind turbine blade is subjected to aerodynamic loads, gravitational loads, inertial loads, centrifugal loads and operational loads due to actions of the control system. For modern large-scale wind turbine blades, a curved blade geometry and utilization of composite materials can cause complicated structural coupling between the flapwise or edgewise bending and twist. These coupling effects have a considerable influence on the aero-elastic responses [30] and can lead to large and complex deformation of blades. Therefore, blade deflections and structural dynamic responses are of great concern. In this part, the tip deflections of 10MW FOWT blades under different environmental conditions are analyzed.

Figures 11 and 12 show the edgewise and flapwise blade tip deflections from two different structural models. Considering the periodic motion and symmetric configuration of the rotating blades, the results of blade 1 is displayed to represent the structural responses of the blades. From these two figures, an apparent difference between the results of the two different models is visible.

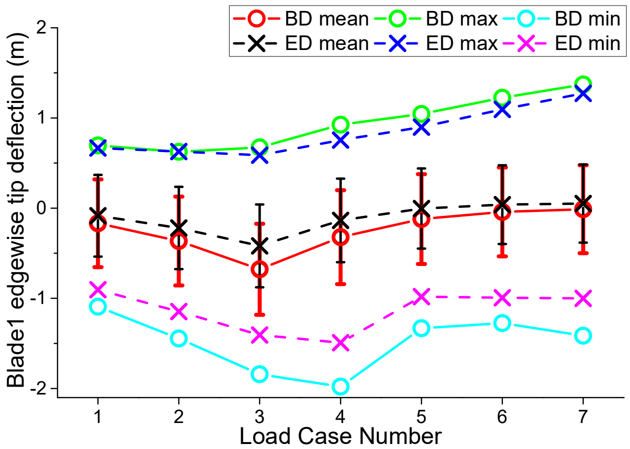

Figure 11 Statistical data of blade 1 edgewise tip deflections

The difference of mean value for the blade edgewise tip deflections between the two models exceeds 50% at all LCs, see Figure 11. The most significant difference can be found in LC5, where the mean value of edgewise tip deflection predicted by BeamDyn module is -0.121m, however, it is only -0.004m by ElastoDyn module. The relative difference is larger at high wind speeds than other LCs. In ElastoDyn module, only the first order edgewise mode was used to predict the deflections of blades. Through the results, we can find that the only edgewise mode cannot accurately predict the blade tip deformation, especially at high wind speeds. Thus, high order modes should be considered for large-scale wind turbine blades.

From Figure 12 the flapwise blade tip deflections can be studied. The results exhibit a good agreement at low wind speeds. It proves that using the first two orders flapwise modes can give a relatively accurate prediction of blade tip deflections at low wind speeds. At high wind speeds, the mean value of ElastoDyn results is larger than BeamDyn's. The largest difference can be found in LC7, the prediction of BeamDyn is -0.447m while for ElastoDyn, it is only -0.064m. It is due to the difference of blade pitch angle and the bend-twist coupling effect. In addition, it is necessary to point out that the maximum flapwise and edgewise tip deflection appears around rated wind speed.

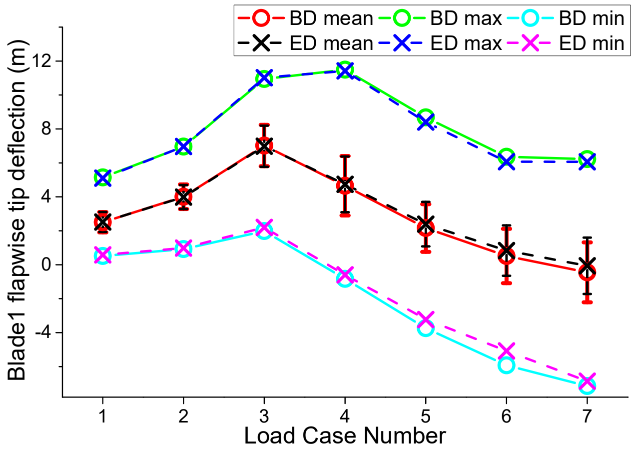

Figure 12 Statistical data of blade 1 flapwise tip deflections

In Figure 11 and 12, it is shown that the absolute value of maximum and minimum blade deflections of BeamDyn is larger than ElastoDyn. At the same time, the mean value of blade tip deflections predicted by BeamDyn module changes more than ElastoDyn as wind speed increases. In other words, BeamDyn module is more sensitive to wind speed. It is due to the utilization of GEBT, which can capture the blade deflections as a function of wind speed more timely and accurately.

6.2.2 Spectral comparison

The power spectral densities (PSDs) of the blade tip deformations are presented in Figures 13 and 14 for different environmental conditions. In each figure, the frequency domain results at below rated (LC2), around rated (LC4) and above-rated (LC6) mean hub-height inflow wind speeds are presented from top to bottom. Each PSD plot is obtained by Fast Fourier Transformation (FFT) based on the average of five independent time series under the same LC. Through these plots, the difference between the two structure models can be analyzed in the frequency domain. The key frequencies, which are highlighted in the former research studies [33, 41] can also be found in the PSDs of the present study. This further proves the accuracy of the numerical models established in this study.

At LC2, the mean wind speed is below rated wind speed and the rotor speed is only 6 rpm (0.1 Hz). In Figure 13a and 14a, the peaks at frequencies of 0.1 Hz, 0.2 Hz and 0.3

Hz are related to the rotor rotation and marked as 1P, 2P, and 3P, respectively. At rated and above rated wind speed, due to the regulation of control system, the rotor speed keeps as a constant of 9.6 rpm (0.16 Hz). The corresponding peaks at 0.16 Hz, 0.32 Hz and 0.48 Hz can be found in Figures 13b, 13c, 14b and 14c. There are not much difference between these two structural models regarding the prediction of aforementioned frequencies.

While the main difference between the two models can be found in the PSDs of edgewise blade tip deflection at high frequencies in Figure 13. The peak around 1 Hz seems to be the 1st blade edgewise mode in panels (a) to (c). According to the results listed in Table 4, the BeamDyn result is more close to the 1st blade edgewise mode, however, the ElastoDyn result is a little higher. Furthermore, the peaks at 1.8 Hz of BeamDyn and 2 Hz of ElastoDyn are most likely to be the blade edge coupled with the drivetrain torsional mode according to reference [33, 41]. The most significant difference can be found at the peak of BeamDyn result around 2.8 Hz which represents the 2nd blade edgewise mode according to the results in [42]. The absence of this peak in ElastoDyn result reveals the advantage of BeamDyn module in capturing the high-frequency component.

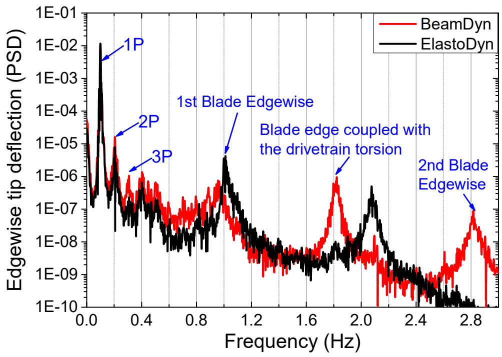

(a) PSD of the edgewise blade-tip deflection under Load Case 2

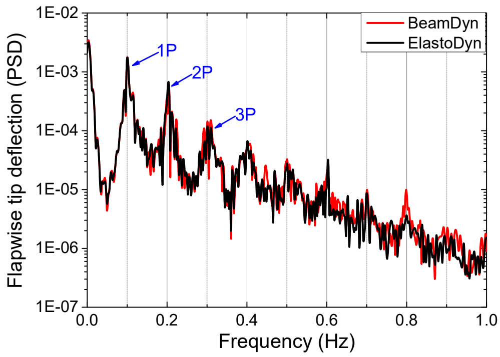

(a) PSD of the flapwise blade-tip deflection under Load Case 2

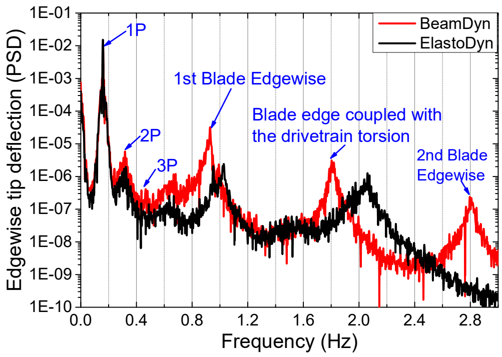

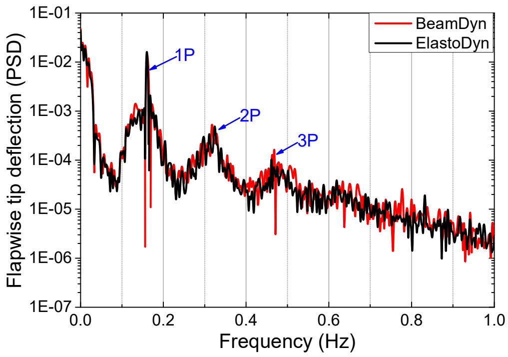

(b) PSD of the edgewise blade-tip deflection under Load Case 4

(b) PSD of the flapwise blade-tip deflection under Load Case 4

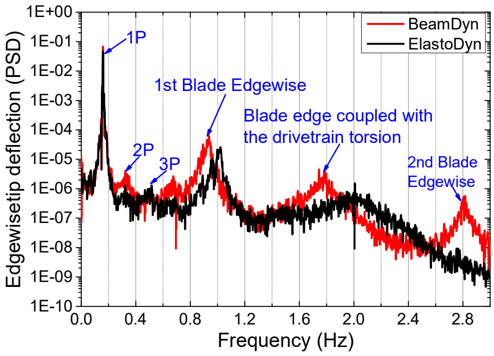

(c) PSD of the edgewise blade-tip deflection under Load Case 6

Figure 13 PSDs of the edgewise blade-tip deflection

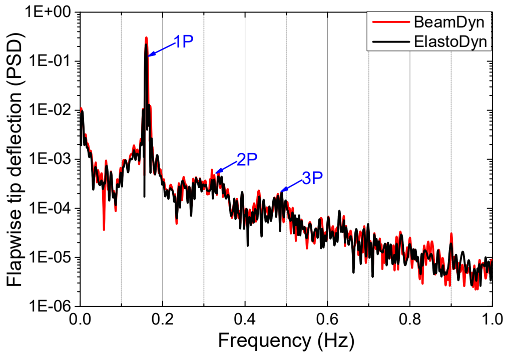

(c) PSD of the flapwise blade-tip deflection under Load Case 6

Figure 14 PSDs of the flapwise blade-tip deflection

6.3 Comparison of blade root bending moment

6.3.1 Statistical results

Both edgewise and flapwise blade root bending moment can be found in Figures 15 and 16 respectively. Because the mean value and standard deviation of edgewise root bending moment are not at the same order of magnitude, an enlarged graph of the mean values of LC4-7 was added in Figure 15. There is seldom apparent difference between these two structural models for the mean values and standard deviations at LC1-3. However, a considerable deviation can be observed at high wind speeds in the mean, maximum and minimum value in Figure 15. At LC7, the mean value of edgewise root bending moment obtained by BeamDyn is 194.75 kN·m. While the result is -43.53 kN·m calculated by ElastoDyn, which is about 4 times smaller than BeamDyn result. In addition, the maximum and minimum value of blade root edgewise bending moment also exhibit an apparent difference at high wind speeds.

As we all know, the edgewise blade root bending moment are primarily dominated by the projection of gravity, from global coordinate to the blade local coordinate. The value of blade pitch angle and torsional deformation directly affects the transformation of these two coordinates and the value of projecting component of gravity. Thus, the differences found at high wind speeds are mainly caused by the diverse component of gravity.

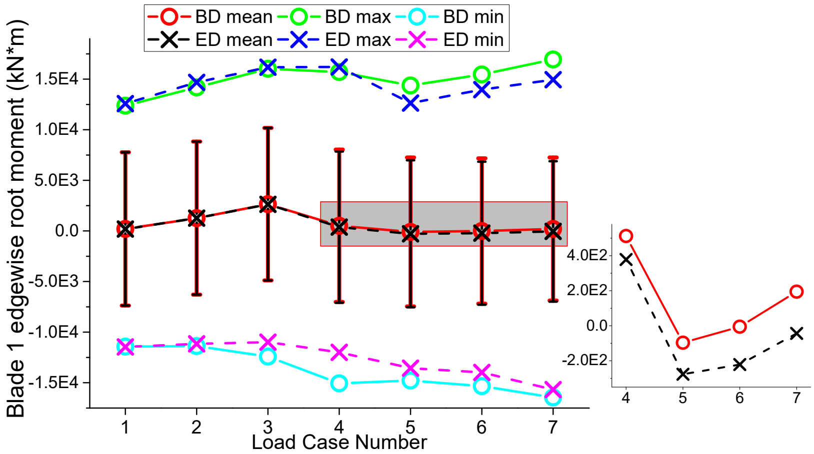

Figure 15 Statistical data of edgewise blade 1 root bending moment

According to Figure16, it can be observed that the results at low wind speeds are almost the same for the two structural models, while a small difference of the mean and maximum value is discernible at high wind speeds. The overall difference for mean value of these two models is below 5%. The flapwise blade root bending moment is determined by the aerodynamic loads. The blade torsional deformation is closely related to the angle of attack and further affect the aerodynamic load. This effect is more pronounced at high wind speeds. Therefore, the lack of torsion deformation in ElastoDyn module leads to the minor difference at high wind speeds.

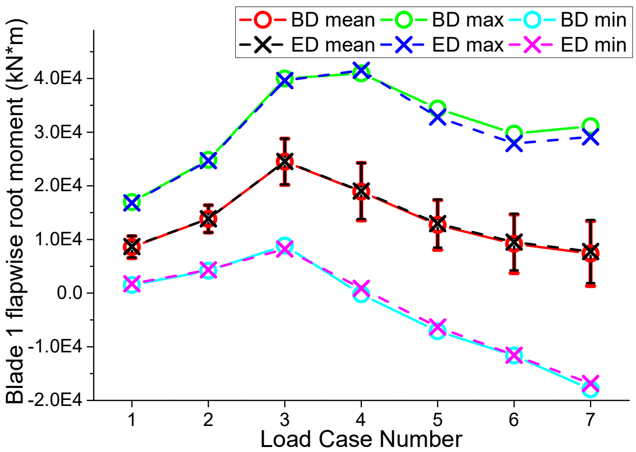

Figure 16 Statistical data of flapwise blade 1 root bending moment

Figure 17 shows the results of blade pitching moment at blade root calculated by the two models. A significant difference is visible between BeamDyn and ElastoDyn results.

The most obvious difference can be found in LC3, where the mean value of BeamDyn is $51.09\,\mathrm{kN\cdot m}$, but for ElastoDyn it is only $5.10\,\mathrm{kN\cdot m}$. The mean value of BeamDyn result is about ten times higher than ElastoDyn. The diversity between these two modules is more apparent around rated wind speeds and higher wind speeds, where the pitch control system begin to work. Thus it can be concluded that the blade structural model has a direct effect on the pitch control system. In future study about pitch control mechanism, BeamDyn module is more recommended for a more precise prediction of blade root reaction moment.

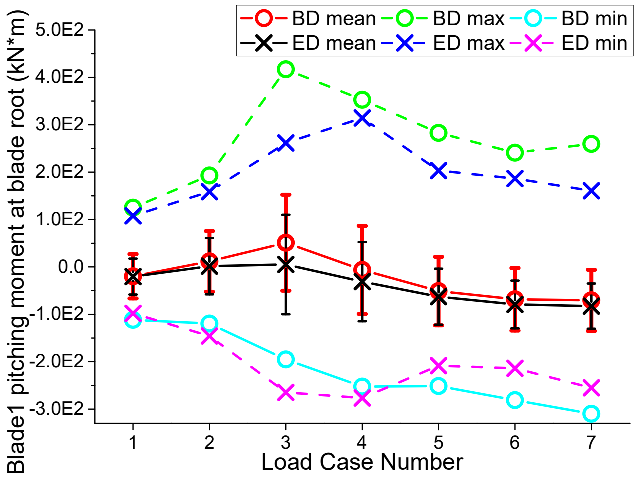

Figure 17 Statistical data of blade pitching moment at blade root

6.3.2 Spectral comparison

The PSDs of blade root bending moment under different environmental conditions are shown in Figures 18 and 19. From Figure 18, the 1P and 2P rotational frequencies can be captured by the two models accurately. But the two models show different peaks at high-frequency region. BeamDyn module predicts a smaller and more precise 1st blade edgewise frequency than ElastoDyn module. The peaks around 2Hz of the two models in figure 18a and 18b are inferred to be a coupled blade in-plane and torsion mode [33]. Like the PSDs of blade tip edgewise deflection, the 2nd blade edgewise mode can be observed in the BeamDyn results instead of ElasoDyn's. From Figure 19, it can be concluded that the PSDs of blade root flapwise bending moment have a similar trend for the two different structural models. The frequencies related to the highest energy are 1P, 2P, and 3P rotational frequencies.

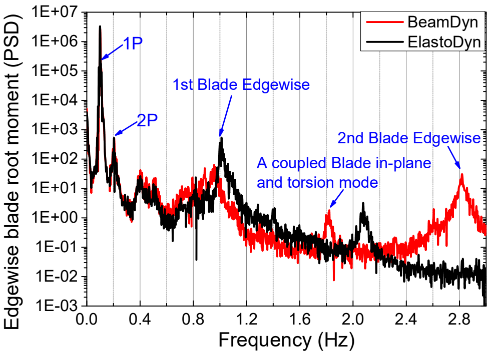

(a) PSD of the edgewise blade-root bending moment under Load Case 2

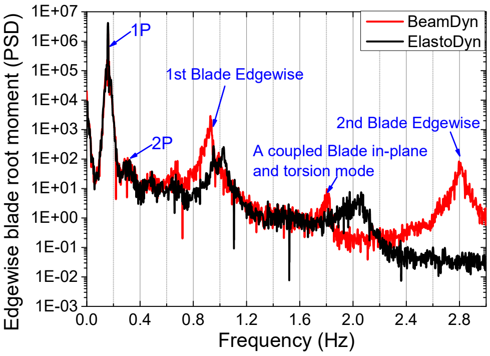

(b) PSD of the edgewise blade-root bending moment under Load Case 4

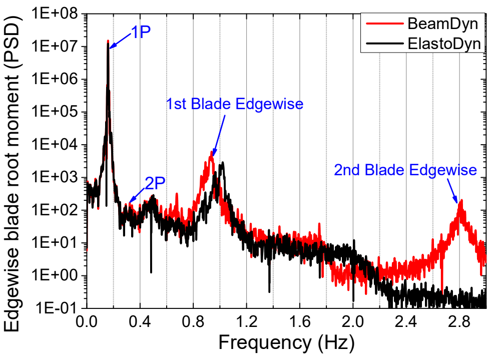

(c) PSD of the edgewise blade-root bending moment under Load Case 6

Figure 18 PSDs of the edgewise blade root bending moment

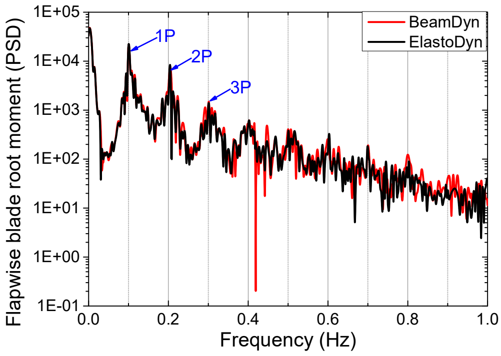

(a) PSD of the flapwise blade-root bending moment under Load Case 2

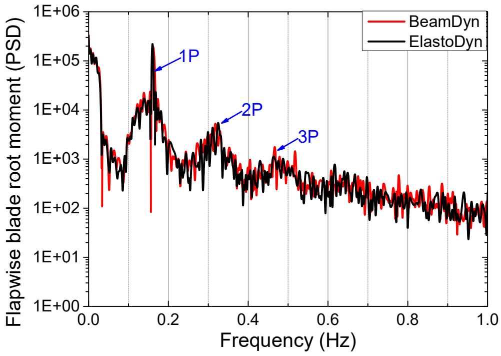

(b) PSD of the flapwise blade-root bending moment under Load Case 4

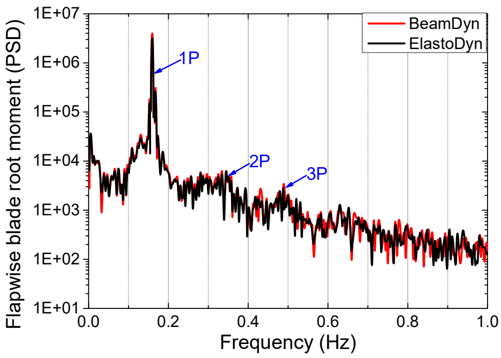

(c) PSD of the flapwise blade-root bending moment under Load Case 6

Figure 19 PSDs of the flapwise blade root bending moment

6.3.3 Extreme blade root bending moments of FOWT

The 1h extreme blade root bending moments under different environmental conditions were extrapolated based on the mean up-crossing rate method as introduced in Section 3.3. Due to the nonlinear nature of FOWT system, the blade structural responses are most likely non-Gaussian under stochastic wind and wave loads. The up-crossing rate method performs better for both Gaussian and non-Gaussian responses in comparison with the global maxima and Weibull tail method [43].

Figures 20 and 21 show one of the example time historis of blade root bending moment dynamic responses at LC7. Figures 22 and 23 show the extrapolation results at LC7 based on the two different blade structural models respectively. The red line in each panel represents the sample mean up-crossing rate $\hat{\nu}^{+}(\zeta)$. The mean up-crossing rates of edgewise and flapwise blade root bending moments were calculated using equation (10) according to the time series obtained by Monte-Carlo simulations. The load level has been standardized by the standard deviation of the samples. The black line $\nu_{fit}^{+}(\zeta)$ is the fitted up-crossing rate in the tail region by equation (15). The 90% fractile value of the 1h extreme blade structural responses distribution is evaluated. According to equation (14), the corresponding mean up-crossing rate is 2.927×10^{-5}. The deviation of the results is also evaluated by the 95% confidence interval, which is denoted as CI_+ and CI_-. The comparison of extreme blade root bending moment under different environmental conditions is demonstrated in Figures 24 and 25.

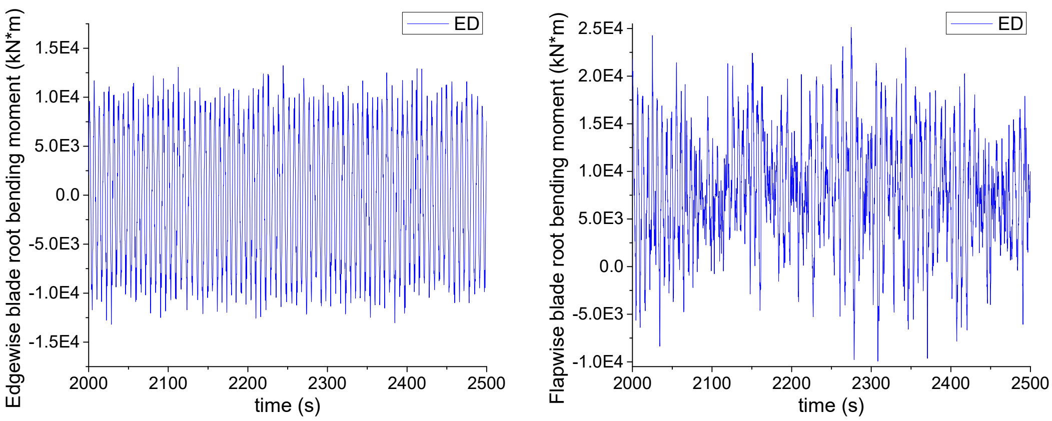

(a) edgewise blade root bending moment (b) flapwise blade root bending moment

Figure 20 The time history of the blade root bending moment at LC7 based on ElastoDyn simulation results

(a) edgewise blade root bending moment (b) flapwise blade root bending moment

Figure 21 The time history of the blade root bending moment at LC7 based on BeamDyn simulation results

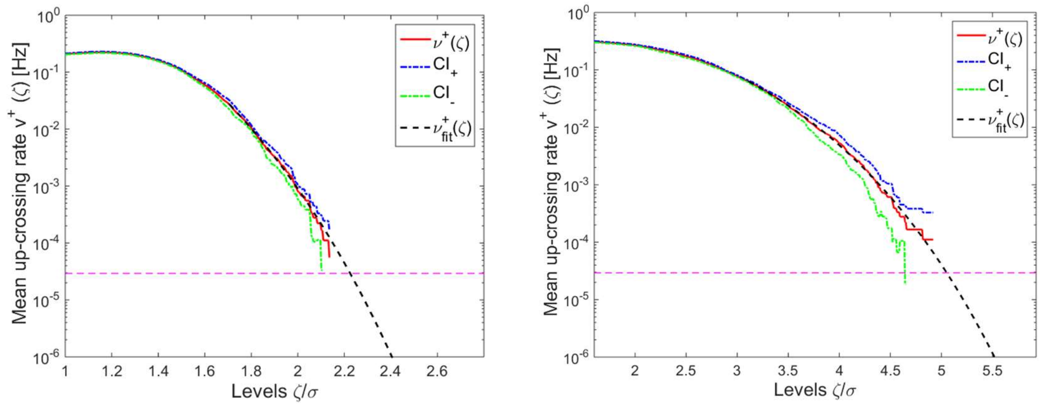

(a) edgewise blade root bending moment (b) flapwise blade root bending moment

Figure 22 The mean up-crossing rate of the blade root bending moment at LC7 based on ElastoDyn simulation results

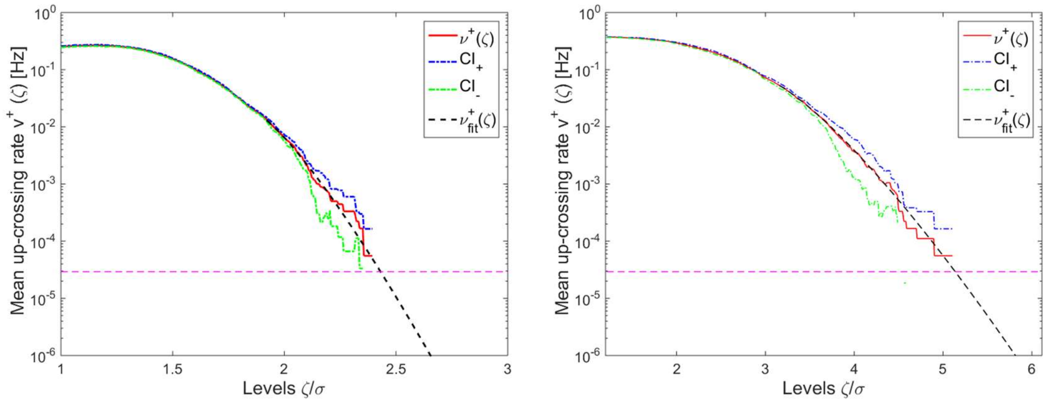

(a) edgewise blade root bending moment (b) flapwise blade root bending moment

Figure 23 The mean up-crossing rate of the blade root bending moment at LC7 based on BeamDyn simulation results

From Figure 24, it can be observed that BeamDyn module predicts the largest 1h extreme edgewise blade root bending moment at LC7, which is 1.717×10^{4} kN·m, however, the result is 1.641×10^{4} kN·m by ElastoDyn module at LC4. Moreover, at low wind speeds, the extreme structural responses estimated by BeamDyn module is smaller than ElastoDyn module. But the difference is not obvious at LC1-4. While BeamDyn module gives relatively higher results at high wind speeds, as shown in Figure 24. The difference of the results are all above 10% at LC5-7. Especially for LC5, the difference between the extreme values estimated by the two structural models is as high as 13.8%. Therefore, the extreme edgewise blade root bending moment may be underestimated, if the ElastoDyn module is implemented at high wind speeds.

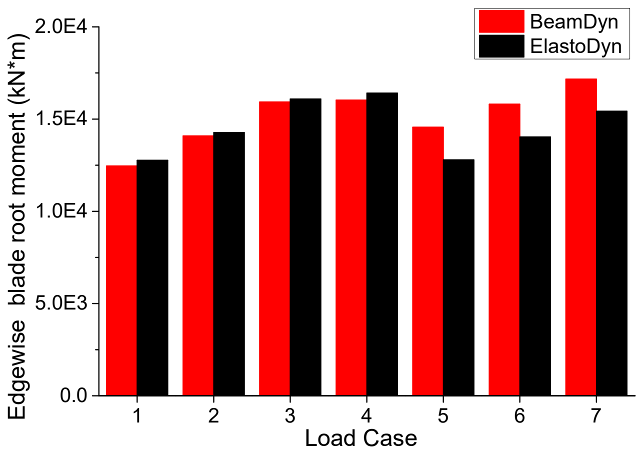

Figure 24 The 90% fractile value of 1h extreme edgewise blade root bending moment

The 90% fractile value of 1h extreme flapwise blade root bending moments are shown in Figure 25. The largest 1h extreme structural responses are observed at LC4 for both of the two models. The extrapolated extreme value is 4.261×10^{4} kN·m based on BeamDyn module, and 4.144×10^{4} kN·m by ElastoDyn module. At all load cases, the extreme flapwise blade root bending moment calculated by BeamDyn module is higher than ElastoDyn module. But the differences between these two models are smaller than 5% at all load cases. Thus it can be concluded that the torsional deformation has a little effect on the prediction of flapwise extreme blade root bending moments.

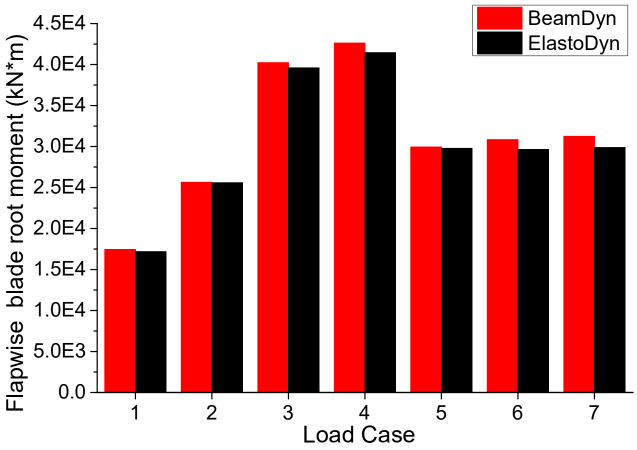

Figure 25 The 90% fractile value of 1h extreme flapwise blade root bending moment

6.3.4 Short-term DELs for blade root bending moments

The short-term fatigue damage at blade root is represented by the damage equivalent loads which are calculated according to Section 3.4. The 1Hz damage equivalent fatigue loads for the edgewise and flapwise blade root bending moment are shown in Figure26 and 27, respectively.

In Figure26, it can be found that at low wind speeds, the two structural models show little difference of 1Hz DELs for edgewise blade root bending moment. However, at high wind speeds, the difference between the two modules are discernible. The maximum 1Hz DELs obtained by the two structural models are both at LC7. The 1Hz DELs calculated based on BeamDyn time-series is 2.004×10^{4} kN·m at LC7, while it is 1.872×10^{4} kN·m for ElastoDyn module. Furthermore, all of the fatigue loads obtained by BeamDyn module are larger than ElastoDyn module, except for LC2. It is noteworthy that the overall tendency of the 1Hz DELs basically maintains unchanged under varied environmental conditions. It is for the reason that the oscillation of edgewise blade root bending moment is mainly affected by the component of gravity which is unchanged under different LCs.

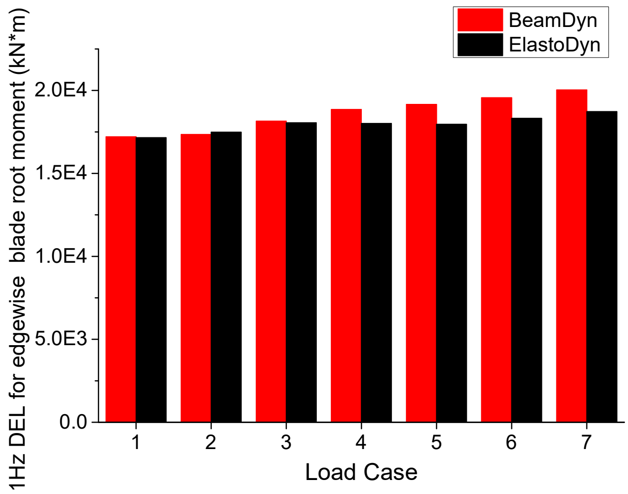

Figure 26 1Hz DEL for edgewise blade root bending moment

The 1Hz DELs for flapwise blade root bending moment are shown in Figure27. Similar to the edgewise fatigue load results, the 1Hz DELs evaluated by the two structural models show good agreement at low wind speeds but diverse from each other at high wind speeds. However, in contrast to the edgewise DELs, the fatigue loads for flapwise blade root bending moment increases apparently as wind speed becoming larger. The largest 1Hz DELs were observed at LC7, and the values are 2.271×10^4 kN·m and 2.180×10^4 kN·m estimated by BeamDyn and ElastoDyn module respectively. Moreover, the fatigue loads calculated based on BeamDyn are larger than ElastoDyn over all the load cases.

Through the comparison, it is evident that the short-term fatigue loads evaluated based on BeamDyn module is larger than ElastoDyn at almost all load cases. Thus it can be inferred that the ElastoDyn blade structural model may underestimate the life time fatigue loads for long-term prediction and give a relatively longer service life than the actual value.

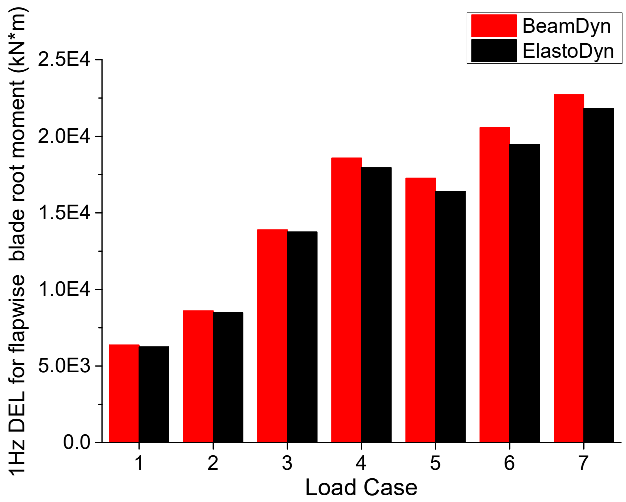

Figure 27 1Hz DEL for flapwise blade root bending moment

7. Conclusions and future work

In this work, two different blade structural models are used to study the dynamic responses of a large-capacity FOWT. Based on the simulation results, the short-term extreme load responses as well as the fatigue damage are further predicted. The numerical models of DTU 10MW RWT mounted on a semi-submersible floating platform are established by adopting the aero-elastic engineering analysis tool OpenFAST. The two different structural modules, ElastoDyn and BeamDyn, which are based on the linear mode superposition method and GEBT respectively, are both used to analyze the global dynamic structural responses of the wind turbine system.

Based on the study, it can be concluded that the fundamental difference between the two structural models is the capacity for predicting large and complicated deformation of rotating blades. According to the dynamic performance simulations, it shows that the two models perform similarly in the prediction of the overall system responses, such as electrical generator power and rotor thrust. When we study on these quantities in the future, the ElastoDyn module is recommended for saving computation time. While, if the blade tip deformation, pitch angle as well as the high-frequency responses are the major focus, the high-fidelity BeamDyn module is more preferred, especially under the high-wind-speed scenarios, according to the simulation results.

Besides, the short-term extreme blade root bending moments and fatigue damages at blade root are calculated and compared. The difference of extreme flapwise bending moments between these two models is not distinctive. However, for edgewise results, the largest extreme values are observed in different cases. At high wind speed cases, the difference of the results are all above 10%, which further indicates that the extreme structural responses may be underestimated if the ElastoDyn module is employed at high wind speeds. Considering the results of fatigue loads, the 1Hz damage equivalent loads predicted by BeamDyn module have larger values than the ElastoDyn ones at almost every LCs. In other words, the implementation of ElastoDyn module may underestimate the life-time fatigue loads for long-term prediction.

Although our simulations are performed based on a specific 10-MW FOWT as an example, the results have much more general implications. Firstly, in the preliminary design of the FOWT system, when the global responses are of concern, the linear mode superposition method should be employed in consideration of computation efficiency. While, in the study of blade strength analysis and fatigue damage evaluation, which are closely associated with the blade dynamic responses under extreme environmental conditions, the high-fidelity GEBT model should be employed for a more accurate prediction. Even though the blade tip deflections and blade root bending moments as well as the short-term fatigue damage at blade root are all analyzed in the present work, the study of the stress distribution along the whole blade, bend-twist coupling effect and the long-term fatigue life estimation for the large-scale wind turbine blades should be included in the future work.

Acknowledgments

The paper was financially supported by Nation Natural Science Foundation of China (Project No. 51879144), and Project funded by China Postdoctoral Science Foundation (No.2019M651042). These sources of support are gratefully acknowledged. The support provided by China Scholarship Council (CSC No. 201706250069) during a visit of Xiaoqi Qu to NTNU is acknowledged. The author also wants to appreciate Adam Wise from NTNU for the discussion of recompiling the control system for a 64-bit application.

Reference

1. *GWEC-Global-Wind-Report-2018*. 2019, GLOBAL WIND ENERGY COUNCIL.
2. Qu, X., et al., *An Analytical Model of Floating Offshore Wind Turbine Blades Considering*

Bending-Torsion Coupling Effect, in *ASME 2018 37th International Conference on Ocean, Offshore and Arctic Engineering*. 2018: Madrid, Spain.

3. Bauchau, O.A., *Flexible Multibody Dynamics*. Solid Mechanics and Its Applications. 2011.
4. Wang, L., et al., *A mathematical model for calculating cross-sectional properties of modern wind turbine composite blades.* Renewable Energy, 2014. **64**: p. 52-60.
5. V.A. Fedorov, N.D., C. Berggreen, S. Krenk, K. Branner and P. Berring, *Iinvestigation of structural behavior due to bend-twist couplings in wind turbine blades*, in *Proceedings of the 17th International Conference of Composite Materials (ICCM)*. Edinburgh, UK.
6. Chen, J., et al., *Coupled aero-hydro-servo-elastic methods for floating wind turbines.* Renewable Energy, 2019. **130**: p. 139-153.
7. Karimi, B. and H. Moradi, *Nonlinear kinematics analysis and internal resonance of wind turbine blade with coupled flapwise and edgewise vibration modes.* Journal of Sound and Vibration, 2018. **435**: p. 390-408.
8. Garrad Hassan and Partners Ltd. *Bladed theory manual v4.7*, 2015.
9. Jason M. Jonkman, M.L.B.J., *FAST User's Guide*. 2005, National Renewable Energy Laboratory.
10. Rezaei, M.M., et al., *Aeroelastic analysis of a rotating wind turbine blade using a geometrically exact formulation.* Nonlinear Dynamics, 2017. **89**(4): p. 2367-2392.
11. Rezaei, M.M., H. Zohoor, and H. Haddadpour, *Aeroelastic modeling and dynamic analysis of a wind turbine rotor by considering geometric nonlinearities.* Journal of Sound and Vibration, 2018. **432**: p. 653-679.
12. Wang, Q., et al., *BeamDyn: a high-fidelity wind turbine blade solver in the FAST modular framework.* Wind Energy, 2017. **20**(8): p. 1439-1462.
13. Zhou, X., K. Huang, and Z. Li, *Geometrically nonlinear beam analysis of composite wind turbine blades based on quadrature element method.* International Journal of Non-Linear Mechanics, 2018. **104**: p. 87-99.
14. Barlas, T., et al., *Extreme load alleviation using industrial implementation of active trailing edge flaps in a full design load basis.* Journal of Physics: Conference Series, 2016. **753**.
15. Graf, P., et al., *Adaptive stratified importance sampling: hybridization of extrapolation and importance sampling Monte Carlo methods for estimation of wind turbine extreme loads.* Wind Energy Science, 2018. **3**(2).
16. International Electrotechnical Commission. *IEC 61400-3 Wind Turbines Part3: Design Requirements for Offshore Wind Turbines. International Electrotechnical Commission: Geneva, Switzerland (2009).*
17. Barone, M., et al., *Decades of Wind Turbine Load Simulation*, in *50th AIAA Aerospace Sciences Meeting including the New Horizons Forum and Aerospace Exposition*. 2012.
18. Xia, Y. and Y. Wang, *Calculation of Out-of-Plane Bending Moment at the Blade Root of Offshore Wind Turbines by Statistic Extrapolation.* Journal of Shanghai Jiaotong University, 2013. **47**(12): p. 1968-1973.
19. International Electrotechnical Commission. *IEC 61400-1 Wind turbines Part 1: Design requirements. International Electrotechnical Commission (2005).*
20. Lott, S., P.W. Cheng, and Iop, *Load extrapolations based on measurements from an offshore wind*

turbine at alpha ventus, in *Science of Making Torque from Wind*. 2016.

21. Cao, Y., V.M. Zavala, and F. D'Amato, *Using stochastic programming and statistical extrapolation to mitigate long-term extreme loads in wind turbines.* Applied Energy, 2018. **230**: p. 1230-1241.
22. Sultania, A. and L. Manuel, *Reliability analysis for a spar-supported floating offshore wind turbine.* Wind Engineering, 2018. **42**(1): p. 51-65.
23. Cheng, Z., et al., *A comparison of extreme structural responses and fatigue damage of semi-submersible type floating horizontal and vertical axis wind turbines.* Renewable Energy, 2017. **108**: p. 207-219.
24. Li, L., et al., *Short-term extreme response and fatigue damage of an integrated offshore renewable energy system.* Renewable Energy, 2018. **126**: p. 617-629.
25. Naess, A. and T. Moan, *Monte Carlo Methods and Extreme Value Estimation*, in *Stochastic Dynamics of Marine Structures*. 2012, Cambridge University Press: Cambridge. p. 341-384.
26. Pegalajar-Jurado, A., et al., *Deliverable D4.5 State-of-the-art models for the two LIFES50+ 10MW floater concepts*. 2018, DTU.
27. Christian Bak, F.Z., Robert Bitsche, Taeseong, A.Y. Kim, Lars Christian Henriksen, Anand Natarajan,, and M.H. Hansen, *Description of the DTU 10MW Reference Wind Turbine*. 2013, DTU Wind Energy.
28. Yu, W., K. Müller, and F. Lemmer, *Deliverable D4.2 Public Definition of the Two LIFES50+ 10MW Floater Concepts*. 2018, University of Stuttgart.
29. Pegalajar-Jurado, A., et al., *State-of-the-art model for the LIFES50+ OO-Star Wind Floater Semi 10MW floating wind turbine.* Journal of Physics: Conference Series, 2018. **1104**.
30. Stäblein, A.R., M.H. Hansen, and D.R. Verelst, *Modal properties and stability of bend–twist coupled wind turbine blades.* Wind Energy Science, 2017. **2**(1): p. 343-360.
31. Jonkman, J.M., *Modeling of the UAE Wind Turbine for Refinement of FAST_AD*. 2003, National Renewable Energy Laboratory.
32. Wang, Q., et al., *BeamDyn User's Guide and Theory Manual*. 2016, National Renewable Energy Laboratory.
33. Guntur, S., et al., *A validation and code-to-code verification of FAST for a megawatt-scale wind turbine with aeroelastically tailored blades.* Wind Energy Science, 2017. **2**(2): p. 443-468.
34. Chai, W., et al., *Efficient Monte Carlo simulation and Grim effective wave model for predicting the extreme response of a vessel rolling in random head seas.* Ocean Engineering, 2016. **123**: p. 191-203.
35. Naess, A. and O. Gaidai, *Monte Carlo Methods for Estimating the Extreme Response of Dynamical Systems.* Journal of Engineering Mechanics, 2008. **134**(8): p. 628-636.
36. Hayman, G.J., *MLife Theory Manual for Version 1.00*. 2012.
37. Borg, M., M. Mirzaei, and H. Bredmose, *Qualification of innovative floating substructures for 10MW wind turbines and water depths greater than 50m*. 2015.
38. Saverin, J., et al., *Aeroelastic simulation of multi-MW wind turbines using a free vortex model coupled to a geometrically exact beam model.* Journal of Physics: Conference Series, 2016. **753**.
39. Krieger, A., et al., *LIFES50+ D7.2 Design Basis*. 2015, DNV-GL.
40. Veritas, Det Norske. *DNV-OS-J101-Design of offshore wind turbine structures. Det Norske*

Veritas (2004).

41. Guntur, S., et al., *FAST v8 Verification and Validation for a MW-scale Wind Turbine with Aeroelastically Tailored Blades*, in *34th Wind Energy Symposium*, A.I.o.A.a. Astronautics, Editor. 2016: San Diego, California, USA.
42. Pavese, C., et al., *HAWC2 and BeamDyn: Comparison Between Beam Structural Models for Aero-Servo-Elastic Frameworks*, in *European Wind Energy Association Annual Conference and Exhibition 2015*. 2015: Paris, France.
43. Saha, N., et al., *Short-term extreme response analysis of a jacket supporting an offshore wind turbine.* Wind Energy, 2014. **17**(1): p. 87-104.